

HOKKAIDO UNIVERSITY

Title	Activation cross sections of deuteron-induced reactions on natural chromium up to 24 MeV
Author(s)	Huang, He; Aikawa, Masayuki; Hanada, Yukina et al.
Citation	Nuclear Instruments and Methods in Physics Research Section B: Beam Interactions with Materials and Atoms, 530, 23-28 https://doi.org/10.1016/j.nimb.2022.09.006
Issue Date	2022-11-01
Doc URL	https://hdl.handle.net/2115/93324
Rights	©2022. This manuscript version is made available under the CC-BY-NC-ND 4.0 license http://creativecommons.org/licenses/by-nc-nd/4.0/
Rights(URL)	https://creativecommons.org/licenses/by-nc-nd/4.0/
Type	journal article
File Information	Nucl Instrum Meth B530 23-28.pdf



Hokkaido University Collection of Scholarly and Academic Papers : HUSCAP

Activation cross sections of deuteron-induced reactions on natural chromium up to 24 MeV

He Huang [a], Masayuki Aikawa [a,b,c], Yukina Hanada [a], Hiromitsu Haba [d]

[a] *Graduate School of Biomedical Science and Engineering, Hokkaido University, Sapporo 060-8638, Japan*

[b] *Faculty of Science, Hokkaido University, Sapporo 060-0810, Japan*

[c] *Global Center for Biomedical Science and Engineering, Faculty of Medicine, Hokkaido University, Sapporo 060-8648, Japan*

[d] *Nishina Center for Accelerator-Based Science, RIKEN, Wako 351-0198, Japan*

Abstract

Radioisotopes in the transition elements such as ^{51}Cr and ^{52g}Mn can be used for medical applications. Investigation on the production reactions of such radioisotopes is valuable. Therefore, excitation functions of the ^{nat}Cr(d,x)^{48}V, ^{51}Cr, ^{52g,52m,54}Mn reactions were measured up to 24-MeV deuteron energy. The experiment was performed at the RIKEN AVF cyclotron. Stacked-foil activation method and gamma-ray spectrometry were used for the measurement. The results were compared with previous experimental data and the prediction values of TENDL-2019. Physical thick target yields of ^{51}Cr and ^{52g}Mn were derived from the measured cross sections.

Keyword

Chromium target, Activation products, Deuteron-induced reaction, Excitation function

1. Introduction

Many radioisotopes in the transition elements are being used for medical applications [1]. ^{51}Cr with a half-life of $T_{1/2}$ = 27.8 d, decaying by an electron capture accompanied with the emission of gamma rays of 320 keV. It was used to label red blood cells as a tracer for the measurement of mass and volume of living systems [2, 3]. Compared with the traditional studies, the ^{51}Cr labeled ethylenediamine tetraacetic acid (^{51}Cr-EDTA) is recently attracting the attention of researchers as it can be used for glomerular filtration rate measurement in renal artery stenosis [4]. The ^{51}Cr-labeled albumin can also be used for the detection of protein loss in the gastrointestinal tract [5, 6]. ^{52g}Mn with a half-life of $T_{1/2}$ = 5.6 d decays by electron capture and positron emission. The mean energy of emitted positrons ($E_{\beta^+}^{mean}$ = 244.6 keV; I_{β^+} = 29%) is comparable with that of ^{18}F ($E_{\beta^+}^{mean}$ = 252 keV; I_{β^+} = 97%). Therefore, ^{52g}Mn can be used in positron emission tomography (PET) and make diagnostic images of similar intrinsic spatial resolution with ^{18}F [7]. It has also a metastable state (^{52m}Mn, $T_{1/2}$ = 21.1 min) that decays by isomeric transition (IT: 1.78%) to the ground state and by the electron capture

and beta decay ($\varepsilon+\beta^+$: 98.22%) to ^{52}Cr. Another positron-emitting radioisotope ^{48}V ($T_{1/2}$ = 15.97 d) can be used for tumor imaging since vanadium is one of essential bioelements in animal organs and tissues [8].

In addition to those important medical applications of radioisotopes, chromium behaviors under ion-beam irradiation deserve attention. In fusion reactors, the anti-corrosion coating of chromium and iron-chromium alloy are used [9, 10]. Thus, the ion-induced reactions on chromium are worthy of investigation.

In this paper, we focused on the deuteron-induced reactions on natural chromium targets. The research of deuteron irradiation on chromium can provide necessary data for the production of useful medical radionuclides and other radiocontaminants. Twelve experimental studies of the reactions on natural chromium and those on enriched chromium comparable after normalization [11-22] were found in the literature survey in the EXFOR library [23]. However, the published excitation function data are scattered. Hasan et al. (2021) [24] calculated the cross sections using the theoretical code EMPIRE 3.2.2 [25] and reproduced part of the experimental data. More reliable experimental data are required for such evaluation and practical use in nuclear medicine. Therefore, we aim to contribute with a new set of data for the nuclear reactions involved in the energy range up to 24 MeV.

2. Material and methods

For the measurements of excitation functions of the deuteron-induced reactions on natural chromium targets, we adopted the well-known and established stacked-foil activation technique followed by high resolution gamma-ray spectrometry.

2.1. Target preparation

The target was assembled from foils of nickel-chromium (NiCr) alloy, ^{nat}Ti, and ^{27}Al. The average thickness of each foil was derived from their measured weight and size before the next processing. The NiCr alloy foil (purity: 99.9%, thickness: 16.6 mg/cm^2, Nilaco Corp., Japan) was the main target of our research. The elemental ratio of the foil was analyzed by a scanning electron microscope with an energy dispersive X-ray spectrometer (Hitachi TM4000 Plus II). The measured ratio was Cr 21.5%, Ni 76.7% and Mn 1.71%, respectively. Two ^{nat}Ti foils (purity: 99.6%, thicknesses: 2.31 and 2.35 mg/cm^2, Nilaco Corp., Japan) were used for the ^{nat}Ti(d,x)^{48}V monitor reaction. The ^{27}Al foil (purity: >99%, thickness: 2.17 mg/cm^2, Nilaco Corp., Japan) was used to catch and separate recoiled products.

All the foils were then cut into squares of 8 mm × 8 mm to fit the size of a target holder. To tackle loss of the recoiled products, two same constituent foils of NiCr or Ti were adjacent to each other. Thirteen sets of NiCr-NiCr-Al-Ti-Ti-Al foils were stacked as a target and installed into the target holder, which also served as a Faraday cup. The loss caused by recoiled nuclides of the second foils was assumed to be compensated by that of the first foils. Only gamma spectra from each second foil

were measured.

2.2. Beam information

The target was irradiated by a deuteron beam with an energy of 24 MeV for 30 minutes at the AVF cyclotron in RIKEN. The beam was collimated to a 3 mm diameter, which corresponded to only a small solid angle and limited the loss of secondary electrons in its backward direction. The average intensity was 105 nA, which was measured by the Faraday cup without suppression voltage. The primary energy of the deuteron beam was 24.0±0.1 MeV measured by the time-of-flight method [26]. The attenuation of energy in each foil was calculated by the stopping powers obtained from the SRIM code [27].

To rectify the beam parameters and target thicknesses, cross sections of the monitor reaction were derived. The net counts of the gamma line at 983.5 keV (I_γ = 99.98%) emitted from each second Ti foils were used to derive the cross sections. The derived cross sections were then compared with the recommended data of IAEA [28, 29]. According to the comparison with the data in 2007 [28], the peak amplitude of the excitation function was found to be slightly lower. To fit the peak amplitude, the beam intensity was corrected by -1.1%. The other parameters were adopted without any correction. The cross sections using the corrected parameters were consistent with the recommended values as shown in Fig. 1.

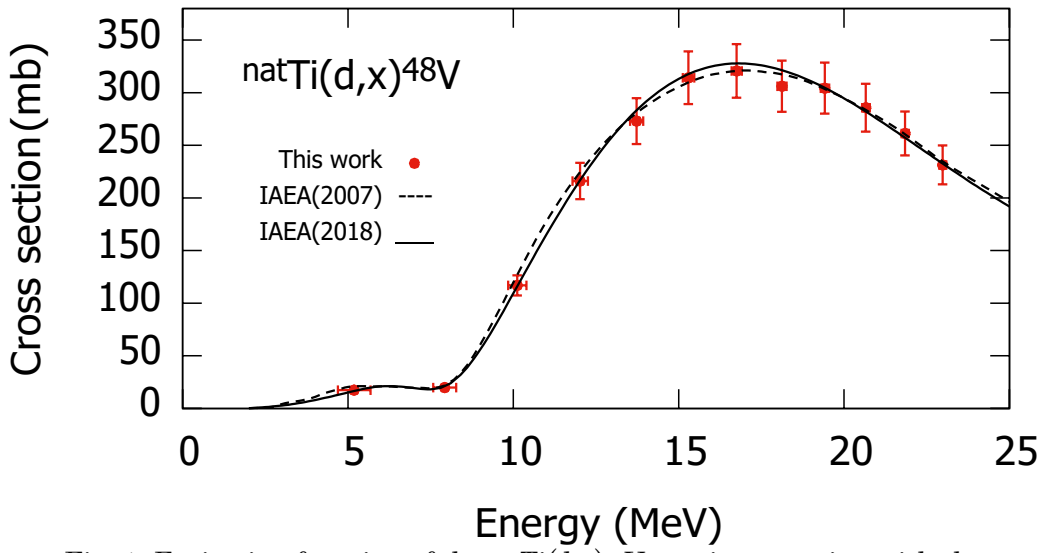


Fig. 1. Excitation function of the ^{nat}Ti(d,x)^{48}V monitor reaction with the recommended values [28, 29].

2.3. Gamma-ray spectrometry

After approximately 1-hour cooling, the irradiated foils were disassembled. Then the gamma-rays emitted from the foils without chemical separation were detected by a high-purity germanium

(HPGe) detector (ORTEC GEM30P4-70). The efficiencies of the detector at different distances were calibrated by a multiple gamma-ray emitting point source consisting of ten radionuclides, ^{57,60}Co, ^{85}Sr, ^{88}Y, ^{109}Cd, ^{113}Sn, ^{137}Cs, ^{139}Ce, ^{203}Hg, and ^{241}Am (Eckert & Ziegler Isotope Products) and an ^{152}Eu standard source (Japan Radioisotope Association). The spectra were analyzed by the analysis software (SEIKO EG&G Gamma Studio).

Seven series of measurements with different cooling times and distances were performed for radionuclides with different half-lives. The dead time of each measurement was kept below 5.2%. The related parameters of each measurement were summarized in Table 1. Produced radionuclides, their characteristic gamma lines, and possible nuclear reactions below 24 MeV are listed in Table 2. The nuclear data were retrieved from the online databases, NuDat 3.0 [30], LiveChart [31], Lund/LBNL Nuclear Data Search [32] and QCalc [33].

Table 1. Measurement information

Series	Distance	Cooling time	Dead time
Ser. 1	5-50 cm	1.5-2.7 h	1.5-2.6%
Ser. 2	5-50 cm	2.8-5.0 h	0.6-1.6%
Ser. 3	5-50 cm	5.2-11.5 h	0.6-1.0%
Ser. 4	5-10 cm	12.0-30.5 h	0.1-3.6%
Ser. 5	5 cm	1.8-2.4 d	0.1-5.2%
Ser. 6	5 cm	10.9-11.3 d	0.0-1.7%
Ser. 7	3 cm	29.9-31.5 d	0.0-1.1%

Table 2. Reaction and decay data retrieved from online databases

Nuclide	Half-life	Decay mode (%)	E_γ (keV)	I_γ (%)	Contributing reaction	Q-value (MeV)	Threshold (MeV)
^{48}V	15.97 d	EC+β^+: 100	**983.53**	99.98	^{50}Cr(d,α)	4.9	0
			511.0	99.8	^{50}Cr(d,p+t)	-14.9	15.5
			1312.106	98.2	^{52}Cr(d,2n+α)	-16.4	-17.0
					^{50}Cr(d,2n+2p)	-23.4	24.3
					^{48}Sc decay		
^{51}Cr	27.7 d	EC: 100	**320.08244**	9.911	^{50}Cr(d,p)	7.0	0
					^{52}Cr(d,2n+p)	-14.3	14.8
					^{53}Cr(d,3n+p)	-22.2	23.0
					^{51}Mn decay		
^{52g}Mn	5.591 d	EC+β^+: 100	1434.092	100.0	^{50}Cr(d,γ)	13.6	0
			935.544	94.5	^{52}Cr(d,2n)	-7.7	8.0
			511	58.8	^{53}Cr(d,3n)	-15.7	16.3
^{52m}Mn	21.1 min	EC+β^+: 98.22	**1434.06**	98.2			
		IT: 1.785	511	193.2			
^{54}Mn	312.20 d	EC+β^+: 100	**834.848**	99.976	^{52}Cr(d,γ)	13.3	0
		β^-: 0.93*10^{-4}			^{53}Cr(d,n)	5.3	0
					^{54}Cr(d,2n)	-4.4	4.5
^{48}V	15.97d	EC+β^+: 100	**983.53**	99.98	^{46}Ti(d,γ)	13.5	0
			511.0	99.8	^{47}Ti(d,n)	4.6	0
			1312.106	98.2	^{48}Ti(d,2n)	-7.0	7.3
					^{49}Ti(d,3n)	-15.2	15.8

2.4. Cross section derivation

To derive the cross sections, the well-known equation was used:

$$\sigma = \frac{N\lambda}{n_T I \varepsilon_d \varepsilon_\gamma \varepsilon_t (1 - e^{-\lambda T_b}) e^{-\lambda T_c} (1 - e^{-\lambda T_m})}$$

where σ is the cross section (cm^2), N is the net count of the characteristic gamma-line, λ is the decay constant of the radioisotope (s^{-1}), n_T is the atomic number areal density of the target (cm^{-2}), I is the deuteron-beam intensity (s^{-1}), ε_d, ε_γ, and ε_t are the efficiency of the HPGe detector, gamma-line branching ratio, and dead time correction, respectively. T_b, T_c, and T_m are the irradiation, cooling, and measurement times (s), respectively.

The total relative uncertainty of the cross section was calculated by the square root of the summed squares of each uncertainty, as the following equation:

$$\Delta\sigma = \sqrt[2]{(\Delta n_T)^2 + (\Delta I)^2 + (\Delta p)^2 + (\Delta \varepsilon_d)^2 + (\Delta \varepsilon_\gamma)^2 + (\Delta N)^2}$$

where Δn_T, ΔI, Δp, $\Delta \varepsilon_d$, Δb, $\Delta \varepsilon_\gamma$, and ΔN are the uncertainties coming from target thickness (1%), beam intensity (5%), material purity (1%), detector efficiency (5%), gamma branching ratio (<1.4%), and counting statistics (0.2–23.2%), respectively. The estimated total uncertainty of cross sections is 7.3-24.3%.

3. Results and discussion

The production cross sections we derived including uncertainties are listed in Table 3 and then displayed in Figs. 2-6. The cross sections of each radionuclide were determined using one measurement series with the proper cooling time after checking the consistency of the cross sections among the seven series. Contributions of the reactions on manganese and nickel in the NiCr alloy foils were considered using experimental data [34, 35] and TENDL-2019 [36]. The contributions of the impurities are found to be negligibly small except for the production of ^{54}Mn from ^{55}Mn in the higher energy region.

The former published data [11-22] found in the EXFOR library [23] and theoretical prediction data [36] were also displayed in Figs. 2-6 and compared with ours. Four experimental studies [11-14] provided elemental cross sections, while the others [15-22] provided cross sections on enriched chromium isotopes. The cross sections on enriched targets were normalized to those on natural abundance for comparison. The theoretical prediction data based on TALYS codes were retrieved from the TENDL-2019 library [36].

Table 3. Production cross sections (mb) in the ^{nat}Cr(d,x) reactions.

Energy (MeV)	^{48}V	^{51}Cr	^{52g}Mn	^{52m}Mn	^{54}Mn
23.4±0.1	0.660±0.126	214±16	114±9	107±15	

22.2±0.1	0.509±0.096	156±11	126±10	103±14	
21.1±0.1	0.523±0.127	97.9±7.3	135±10	117±13	
19.8±0.1	0.798±0.139	50.2±4.0	142±11	129±13	
18.6±0.1	0.644±0.154	26.2±2.5	140±10	130±12	
17.2±0.1	1.21±0.16	20.4±2.1	137±10	141±12	
15.8±0.2	1.24±0.13	16.9±1.7	123±9	129±11	
14.3±0.2	1.94±0.18	17.5±1.6	108±8	121±10	
12.6±0.2	2.26±0.23	16.8±1.9	81.1±6.0	85.9±7.1	
10.8±0.3	2.45±0.20	22.8±1.8	38.5±2.8	37.9±3.5	31.5±2.3
8.7±0.3	1.76±0.16	27.1±2.1	1.79±0.14		32.9±2.5
6.2±0.4	0.779±0.072	27.7±2.0			31.7±2.3
2.6±0.9		1.49±0.15			1.34±0.12

3.1. Cumulative formation of the ^{48}V radionuclide

The cumulative cross sections of ^{48}V production were derived using the gamma line at 983.525 keV ($T_{1/2}$ = 15.9735 d; I_γ = 99.98%) after the cooling time of 29.9 days. Its parent nuclide ^{48}Cr ($T_{1/2}$ = 21.56 h) decayed during the cooling time. According to TENDL-2019 [36] , contribution of deuteron-induced reactions on ^{nat}Ni in the NiCr foil is negligible below 24 MeV. The ^{55}Mn(d,2ntα)^{48}V reaction is impossible to occur in this energy region due to its threshold energy of 34.8 MeV. The derived cross sections in Fig. 2 are compared with the former experiment data [12-14, 16, 17, 19, 22] and the theoretical prediction of TENDL-2019 [36]. The former experimental data are consistent with ours. The peak position of TENDL-2019 slightly shifts to the lower energy.

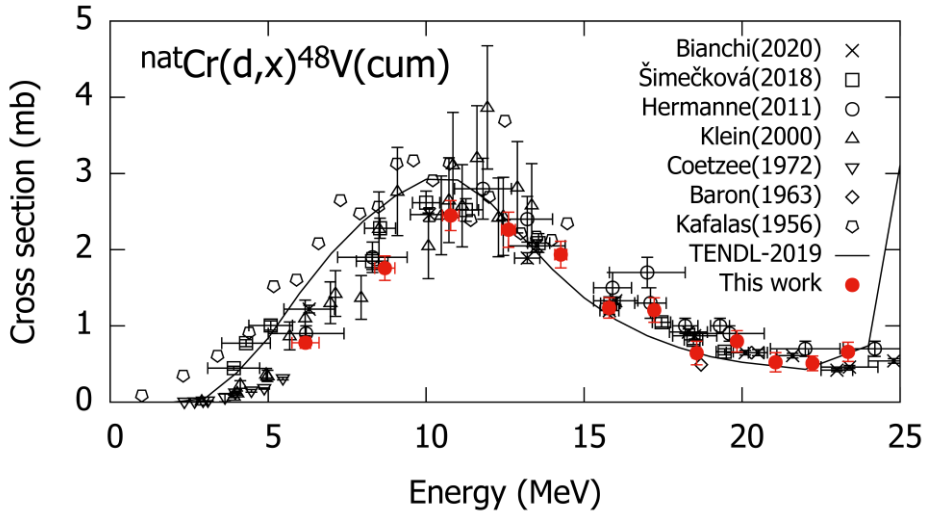


Fig. 2 Cross sections of the ^{nat}Cr(d,x)^{48}V reaction with the previous data [12-14, 16, 17, 19, 22] and the TENDL-2019 [36].

3.2. Cumulative formation of the ^{51}Cr radionuclide

The cumulative cross sections of ^{51}Cr ($T_{1/2}$ = 27.704 d) were determined using spectra measured after a cooling time of 29.9 days. Its parent nuclide ^{51}Mn ($T_{1/2}$ = 46.2 min) simultaneously produced

in the irradiation decayed during the cooling time. The cross sections of the $^{nat}Ni(d,x)^{51}Cr$ reaction in the NiCr alloy foils are negligibly small below 24 MeV according to TENDL-2019 [36]. The experimental cross sections of the $^{55}Mn(d,2n\alpha)^{51}Cr$ reaction are 0.7 and 1.8 mb at 22.1 and 23.8 MeV, respectively [34]. Thus, the contributions from ^{nat}Ni and ^{55}Mn in the NiCr foils are estimated to be less than 1%. The result of our work compared with the former experimental data [11-14, 16, 17, 19] and the theoretical prediction of TENDL-2019 [36] are shown in Fig. 3(a). Since the values in the low-energy region are much smaller than those in the region above 20 MeV, we also draw a graph in a logarithmic scale in Fig. 3(b). Once above 18 MeV, the predicted values of TENDL-2019 much greater than the experimental data.

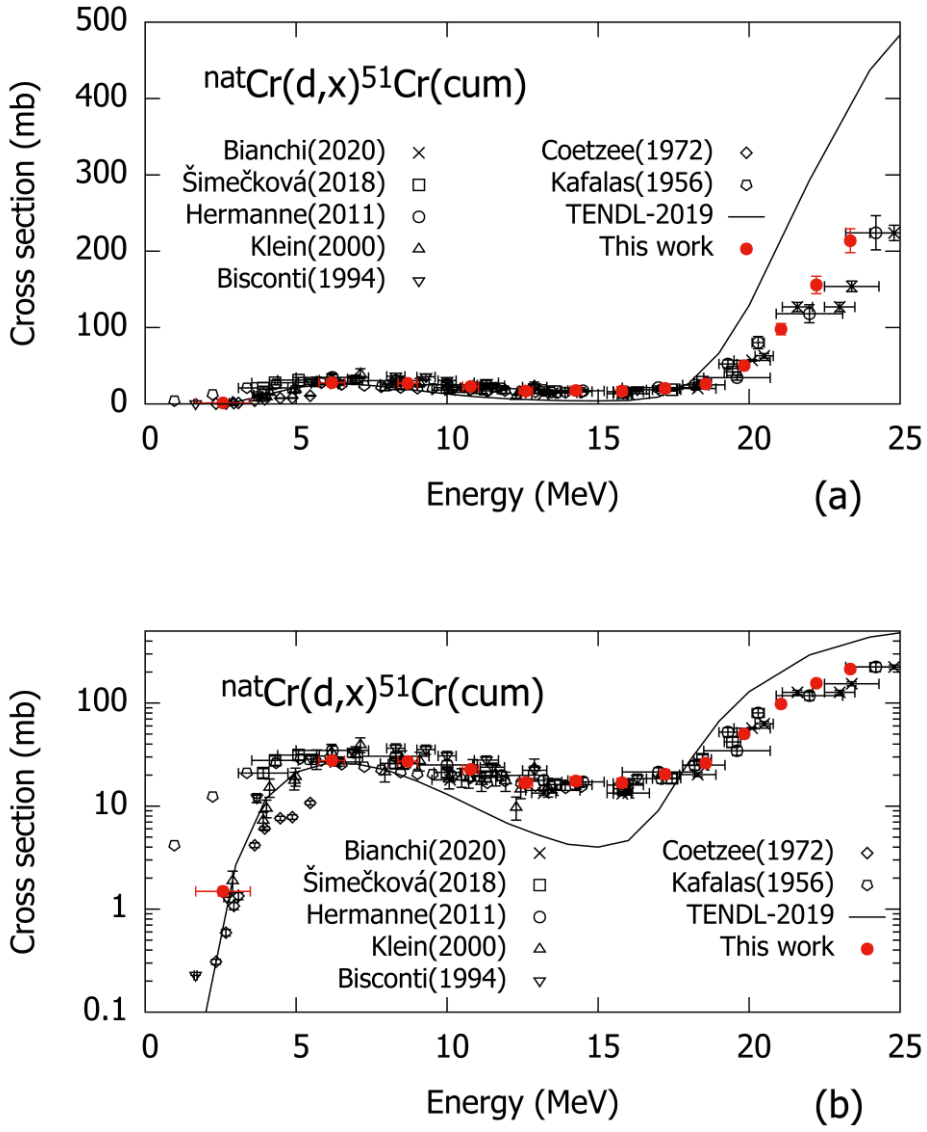


Fig. 3 Cross sections of the $^{nat}Cr(d,x)^{51}Cr(cum)$ reaction with the previous data [11-14, 16, 17, 19] and the TENDL-2019 [36] values, in (a) linear and (b) logarithmic scales.

3.3. Cumulative formation of the ^{52g}Mn radionuclide

^{52g}Mn ($I^{\pi} = 6^{+}$) has a half-life of 5.591 d longer than its metastable state ^{52m}Mn ($I^{\pi} = 2^{+}$) with a rather short half-life of 21.1 min. The branching ratio of the ^{52m}Mn decay to the ground state is only 1.78% by the isomeric transition. The main decay product of ^{52m}Mn is ^{52}Cr by electron capture and positron emission with a branching ratio of 98.22%. In our experiment, the cross sections of ^{52g}Mn were determined after a cooling time of 1.8 days using the gamma line at 935.544 keV (I_{γ} = 94.5%). Therefore, the results contain the small contribution of ^{52m}Mn and show cumulative cross sections. The results are compared with former experimental data [12-15, 17, 18, 20, 21] and the TENDL-2019 values [36] in Fig. 4.

Our data are in agreement with the most recently published data of Bianchi et al. (2020) and Šimečková et al. (2018) and slightly lower than those of Hermanne et al. (2011) above 14 MeV. The theoretical values of TENDL-2019 overestimate the experimental data.

The possible contribution of the ^{55}Mn(d,2nα)^{52g}Mn reaction was estimated to be very small using the experimental values [34], less than 0.02 mb and was neglected. The possible contribution of the ^{nat}Ni(d,x)^{52g}Mn reaction was estimated using the experimental values [35] to be less than 5.3 mb below 24 MeV, and considered to be negligible within our experimental errors.

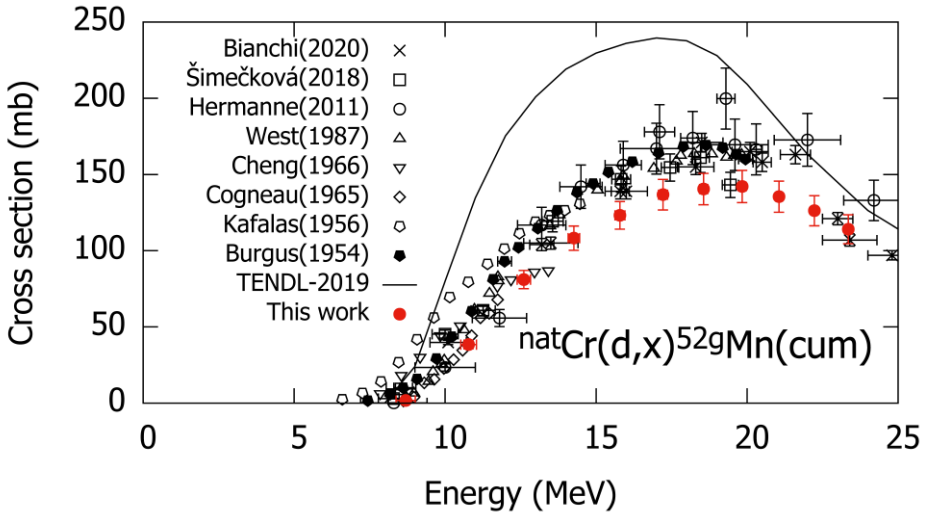


Fig. 4 Cross sections of the ^{nat}Cr(d,x)^{52g}Mn(cum) reaction with the previous data [12-15, 17, 18, 20, 21] and the TENDL-2019 [36] values.

3.4. Formation of the ^{52m}Mn radionuclide

As discussed in section 3.3, ^{52}Mn has a short-lived metastable state ^{52m}Mn. Due to its half-life of only 21.1 min, we measured the gamma line at 1434.06 keV after a short cooling time of 90 min. Since

its ground state ^{52g}Mn also emits 1434.06-keV gamma rays, the contribution of ^{52g}Mn was subtracted. The contribution of ^{52g}Mn was estimated using another gamma line at 935.544 keV (I_γ = 94.5%). The cross sections were determined using the corrected net counts.

Our measured data are compared with the former published data [13, 15, 18] and the TENDL-2019 values [36] in Fig. 5. Our data are larger than those of Šimečková et al. (2018) at the higher energy region. The predicted data of TENDL-2019 are larger than our experimental data below 22 MeV. Our experiment provides the cross sections above 20 MeV for the first time.

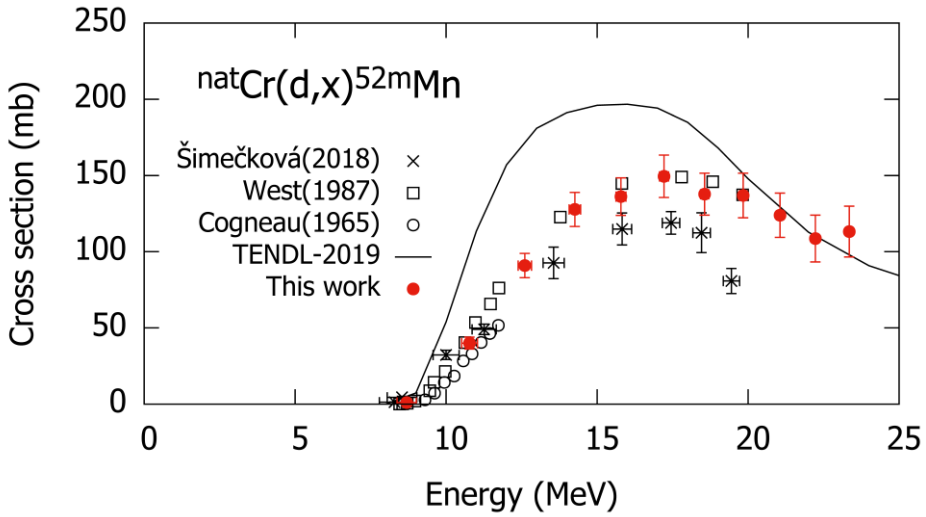


Fig. 5 Cross sections of the ^{nat}Cr(d,x)^{52m}Mn reaction with the previous data [13, 15, 18] and the TENDL-2019 values [36].

3.5. Formation of the ^{54}Mn radionuclide

The activity of ^{54}Mn was derived using the net counts of the gamma line at 834.848 keV. Taking into account the rather long half-life ($T_{1/2}$ = 312.2 d), the measurements were performed after the cooling time of 29.9 days. Because the NiCr alloy foils containing manganese were used as the irradiation target, the yield of ^{54}Mn was affected by ^{nat}Ni and ^{nat}Mn in the high energy region. Based on the threshold energy of the ^{55}Mn(d,nd)^{54}Mn reaction (E_{th} = 10.6 MeV), only data below 10 MeV are shown in Fig. 6. The contributions of the ^{58}Ni(d,2pα)^{54}Mn (E_{th} = 8.8 MeV), ^{60}Ni(d,2α)^{54}Mn (E_{th} = 0.6 MeV) and ^{55}Mn(d,t)^{54}Mn reactions (E_{th} = 4.1 MeV) are expected to be very small according to TENDL-2019 [36] and experimental data [34, 35] although their threshold energies are lower than 10.6 MeV.

Our data are compared with the former experimental data [12-14, 17] and the predicted values of TENDL-2019 [36]. Our result is in good agreement with the experimental data except that of Kafalas et al. (1956).

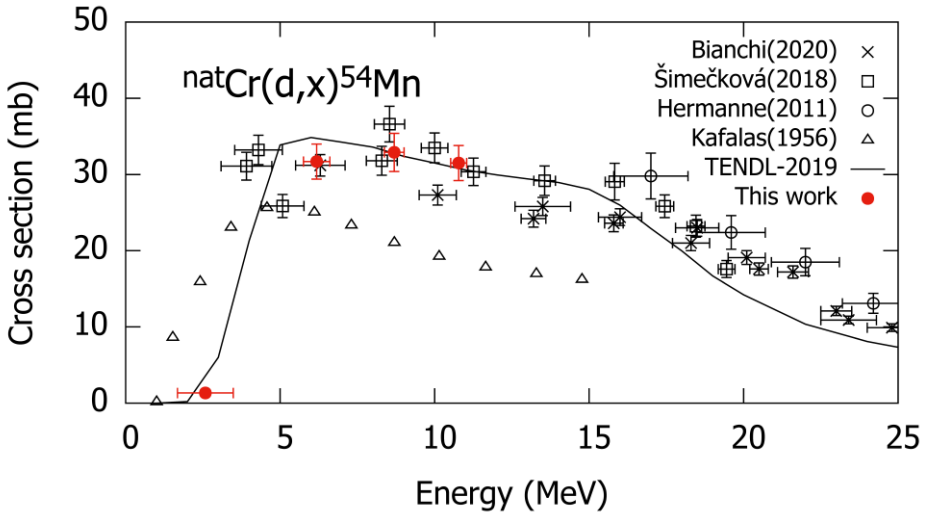


Fig. 6 Cross sections of the ^{nat}Cr(d,x)^{54}Mn reaction with the previous data [12-14, 17] and the TENDL-2019 [36].

3.6. Physical thick target yields of ^{51}Cr, ^{52g}Mn

The physical thick target yields [37] of ^{51}Cr and ^{52g}Mn were derived from our experimental cross section data and compared with the formerly published experimental data in Fig. 7 and Fig. Fig. 8. The former experimental datum of ^{51}Cr measured earlier [38] is lower than our result. The experimental data of ^{52g}Mn [38, 39] measured earlier agree well with our curve.

The yields of ^{51}Cr and ^{52g}Mn can reach 520 MBq/C and 4.9 GBq/C at 23.3 MeV, respectively. The yields may be enough for practical use. However, high specific activities of the products cannot be obtained because of difficult chemical separation of ^{51}Cr from ^{nat}Cr targets and ^{52g}Mn from co-produced longer-lived Mn isotopes. To reduce such contamination, enriched targets or proton-induced reactions are preferable.

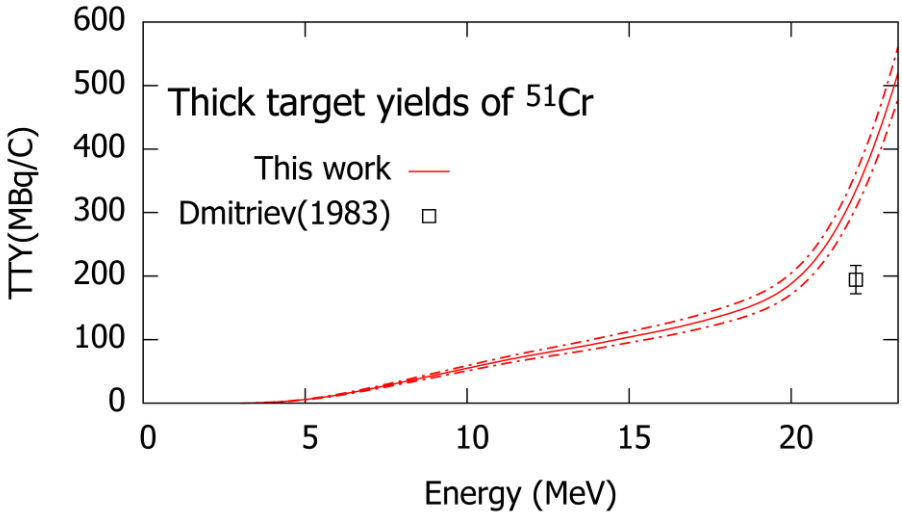


Fig. 7 Thick target yields of ^{51}Cr (sold-line) with their uncertainties (dot-dashed lines) derived by our experiment cross sections and the former published data [38] .

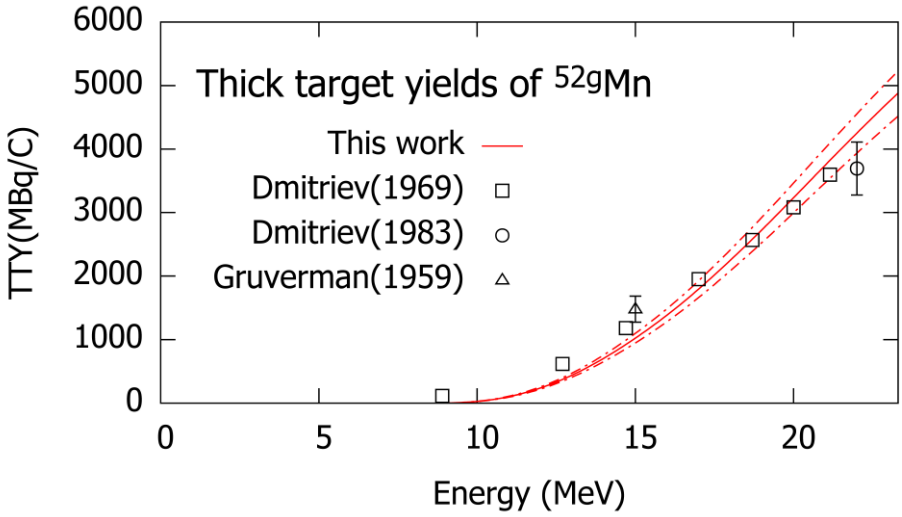


Fig. 8 Thick target yields of ^{52g}Mn (sold-line) with their uncertainties (dot-dashed lines) derived by our experimental cross sections and the former published data [38-40].

4.Summary

The excitation function measurement for the deuteron-induced reactions on natural chromium was performed up to 24 MeV at the RIKEN AVF cyclotron. The stacked-foil activation method and high-resolution gamma-ray spectrometry were used for this experiment. The production cross sections of ^{48}V, ^{51}Cr, ^{52g,52m,54}Mn were measured up to 24 MeV. The data derived by us were compared with the theoretical values of TENDL-2019 and the previously published data. The obtained cross sections are

contributable to the production of medical radioisotopes and development and optimization of nuclear reaction model codes.

Acknowledgment

This work was carried out at RI Beam Factory operated by RIKEN Nishina Center and CNS, University of Tokyo, Japan.

Declarations of interest

None

Reference

1. I.F. Chaple, S.E. Lapi, Production and Use of the First-Row Transition Metal PET Radionuclides ^{43,44}Sc, ^{52}Mn, and ^{45}Ti. J. Nucl. Med. 59(2018) 1655-1659 https://doi.org/10.2967/jnumed.118.213264.
2. S.J. Gray, K. Sterling, The tagging of red cells and plasma proteins with radioactive chromium. J. Clin. Invest. 29(1950) 1604-13 https://doi.org/10.1172/JCI102403.
3. A.B. Willett, V.V. Grantham, Determination of hemolytic anemia through the study of ^{51}Cr red cell survival and splenic sequestration. J. Nucl. Med. Technol. 36(2008) 95-8 https://doi.org/10.2967/jnmt.107.049023.
4. A.A. Chaves, C.A. Buchpiguel, J.N. Praxedes, L.A. Bortolotto, M.T. Sapienza, Glomerular filtration rate measured by (51)Cr-EDTA clearance: Evaluation of captopril-induced changes in hypertensive patients with and without renal artery stenosis. Clinics (Sao Paulo). 65(2010) 607-12 https://doi.org/10.1590/S1807-59322010000600008.
5. T.A. Waldmann, R.D. Wochner, W. Strober, The role of the gastrointestinal tract in plasma protein metabolism. Am. J. Med. 46(1969) 275-285 https://doi.org/10.1016/0002-9343(69)90011-4.
6. R.M. Kerr, J.J. Du Bois, P.R. Holt, Use of ^{125}I- and ^{51}Cr-labeled albumin for the measurement of gastrointestinal and total albumin catabolism. J. Clin. Invest. 46(1967) 2064-2082 https://doi.org/10.1172/JCI105694.
7. M. Pagani, S. Stone-Elander, S.A. Larsson, Alternative positron emission tomography with non-conventional positron emitters: effects of their physical properties on image quality and potential clinical applications. Eur. J. Nucl. Med. 24(1997) 1301-27 https://doi.org/10.1007/s002590050156.
8. I. Kuni, I. Tatsuo, I. Ren, K. Mieko, K. Shuichi, Localizing efficiency of [^{48}V]vanadyl-pheophorbide in tumor as a new tumor imaging agent. Int. J. Radiat. Appl. Instrument. Part B. Nucl. Med. Biol. 16(1989) 783-787,789 https://doi.org/10.1016/0883-2897(89)90162-1.
9. P.P. Liu, R. Yu, Y.M. Zhu, M.Z. Zhao, J.W. Bai, F.R. Wan, Q. Zhan, Deuterium ion irradiation

induced precipitation in Fe–Cr alloy: Characterization and effects on irradiation behavior. J. Nucl. Mater. 459(2015) 81-89 https://doi.org/10.1016/j.jnucmat.2014.12.124.

10. S.J. Zinkle, G.S. Was, Materials challenges in nuclear energy. Acta Mater. 61(2013) 735-758 https://doi.org/10.1016/j.actamat.2012.11.004.
11. R. Bisconti, K. Casteleyn, M. Castiglioni, F. Fossati, L. Manes, M.F. Stroosnijder, Production of ^{51}Cr by deuteron activation of natural chromium. Nucl. Instruments Methods Phys. Res. Sect. B Beam Interact. with Mater. Atoms. 88(1994) 282-286 http://dx.doi.org/10.1016/0168-583X(94)95325-2.
12. F. Bianchi, C. Marchi, G. Fuad, F. Groppi, F. Haddad, L. Magagnin, S. Manenti, On the production of ^{52g}Mn by deuteron irradiation on natural chromium and its radionuclidic purity. Appl. Radiat. Isot. 166(2020) 109329 https://doi.org/10.1016/j.apradiso.2020.109329.
13. E. Šimečková, M. Avrigeanu, U. Fischer, J. Mrázek, J. Novak, M. Štefánik, C. Costache, V. Avrigeanu, Consistent account of deuteron-induced reactions on ^{nat}Cr up to 60 MeV. Phys. Rev. C. 98(2018) https://doi.org/10.1103/PhysRevC.98.034606.
14. A. Hermanne, A.R. R., F. Tárkányi, S. Takács, M. Takács, A. Ignatyuk, Cross sections of deuteron induced reactions on natCr up to 50MeV: Experiments and comparison with theoretical codes. Nucl. Instruments Methods Phys. Res. Sect. B Beam Interact. with Mater. Atoms. 269(2011) 2563-2571 https://doi.org/10.1016/j.nimb.2011.07.008.
15. H.I. West, Jr., R.G. Lanier, M.G. Mustafa, 52Cr(p,n)52Mn^{g,m} and ^{52}Cr(d,2n)^{52}Mn^{g,m} excitation functions. Phys Rev C Nucl Phys. 35(1987) 2067-2076 https://link.aps.org/doi/10.1103/PhysRevC.35.2067.
16. A.T.J. Klein, F. Rösch, S.M. Qaim, Investigation of ^{50}Cr(d,n)^{51}Mn and ^{nat}Cr(p,x)^{51}Mn processes with respect to the production of the positron emitter ^{51}Mn. Radiochimica. Acta. 88(2000) 253-264 https://doi.org/10.1524/ract.2000.88.5.253.
17. P. Kafalas, J.W. Irvine, Nuclear Excitation Functions and Thick Target Yields: (Cr+d). Phys. Rev. 104(1956) 703-705 https://link.aps.org/doi/10.1103/PhysRev.104.703.
18. M. Cogneau, L. Gilly, J. Cara, Absolute cross sections and excitation functions for deuteron induced reactions on chromium between 2 and 12 MeV. Nucl. Phys. 79(1966) 203-208 https://doi.org/10.1016/0029-5582(66)90403-2.
19. P.P. Coetzee, M.A.X. Peisach, Activation Cross Sections for Deuteron-Induced Reactions on some Elements of the First Transition Series, up to 5.5 MeV. Radiochim. Acta. 17(1972) 1-6 https://doi.org/10.1524/ract.1972.17.1.1.
20. W.Z. Cheng Xiaowu, Wang Zhenjie,Yang Jinqing, Some measurements of deuteron induced excitation function at 13 MeV. Acta Phys Sin, (1966) 259
21. W.H. Burgus, G.A. Cowan, J.W. Hadley, W. Hess, T. Shull, M.L. Stevenson, H.F. York, Cross Sections for the Reactions Ti^{48}(d, 2n)V^{48}; Cr^{52}(d, 2n)Mn^{52}; and Fe^{56}(d, 2n)Co^{56}. Phys. Rev.

95(1954) 750-751 https://doi.org/10.1103/PhysRev.95.750.

22. N. Baron, B.L. Cohen, Activation Cross-Section Survey of Deuteron-Induced Reactions. Phys. Rev. 129(1963) 2636-2642 https://link.aps.org/doi/10.1103/PhysRev.129.2636.
23. N. Otuka, E. Dupont, V. Semkova, B. Pritychenko, A.I. Blokhin, M. Aikawa, S. Babykina, M. Bossant, G. Chen, S. Dunaeva, R.A. Forrest, T. Fukahori, N. Furutachi, S. Ganesan, Z. Ge, O.O. Gritzay, M. Herman, S. Hlavač, K. Katō, B. Lalremruata, Y.O. Lee, A. Makinaga, K. Matsumoto, M. Mikhaylyukova, G. Pikulina, V.G. Pronyaev, A. Saxena, O. Schwerer, S.P. Simakov, N. Soppera, R. Suzuki, S. Takács, X. Tao, S. Taova, F. Tárkányi, V.V. Varlamov, J. Wang, S.C. Yang, V. Zerkin, Y. Zhuang, Towards a More Complete and Accurate Experimental Nuclear Reaction Data Library (EXFOR): International Collaboration Between Nuclear Reaction Data Centres (NRDC). Nucl. Data Sheets. 120(2014) 272-276 https://doi.org/10.1016/j.nds.2014.07.065.
24. G. Hasan, E. Nury, F. Bianchi, S. Manenti, F. Groppi, Theoretical cross-sections of deuteron-induced reaction on natural chromium by EMPIRE code for the production of ^{52}Mn, ^{54}Mn, ^{51}Cr and ^{48}V. Radiat. Eff. Defects Solids. 176(2021) 983-994 https://doi.org/10.1080/10420150.2021.1986823.
25. M. Herman, R. Capote, M. Sin, A. Trkov, B.V. Carlson, P. Obložinský, C.M. Mattoon, H. Wienke, S. Hoblit, Y.-S. Cho, G.P.A. Nobre1, V.A. Plujko, V. Zerkin, Empire-32 Malta Modular System for Nuclear Reaction Calculations and Nuclear Data Evaluation User's Manual. International Atomic Energy Agency (IAEA), (2013) 299
26. T. Watanabe, M. Fujimaki, N. Fukunishi, H. Imao, O. Kamigaito, M. Kase, M. Komiyama, N. Sakamoto, K. Suda, M. Wakasugi, K. Yamada, Beam energy and longitudinal beam profile measurement system at the RIBF. in: ,Proc. 5th Int. Part. Accel. Conf. (IPAC 2014), (2014) 3566–3568
27. J.F. Ziegler, J.P. Biersack, M.D. Ziegler. SRIM: the Stopping and Range of Ions in Matter. 2008; Available from: http://www.srim.org.
28. F. Tárkányi, S. Takács, K. Gul, A. Hermanne, M.G. Mustafa, M. Nortier, P. Obložinský, B. S.M. Qaim, Scholten, Y.N. Shubin, Z. Yousiang. Monitor Reactions 2007, updated version of charged particle crosssection database for medical radioisotope production, IAEA-TECDOC-1211. 2007; Available from: https://wwwnds.iaea.org/medical/medical-old/monitor_reactions.html.
29. A. Hermanne, A.V. Ignatyuk, R. Capote, B.V. Carlson, J.W. Engle, M.A. Kellett, T. Kibédi, G. Kim, F.G. Kondev, M. Hussain, O. Lebeda, A. Luca, Y. Nagai, H. Naik, A.L. Nichols, F.M. Nortier, S. V.Suryanarayana, S. Takács, F.T. Tárkányi, M. Verpelli, Reference Cross Sections for Charged-particle Monitor Reactions. Nucl. Data Sheets. 148(2018) 338-382 https://doi.org/10.1016/j.nds.2018.02.009.
30. National Nuclear Data Center, information extracted from the NuDat database, NuDat 3.0.

Available from: https://www.nndc.bnl.gov/nudat/.

31. International Atomic Energy Agency, LiveChart of Nuclides. 2009; Available from: https://wwwnds.iaea.org/livechart/.
32. S.Y.F. Chu, L.P. Ekström, R.B. Firestone. The Lund/LBNL Nuclear Data Search. 1999; Available from: http://nucleardata.nuclear.lu.se/toi/.
33. B. Pritychenko, A. Sonzogni. Q-value Calculator (QCalc). 2003; Available from: http://www.nndc.bnl.gov/qcalc/.
34. F. Tárkányi, F. Ditrói, S. Takács, A. Hermanne, A.V. Ignatyuk, Extension of experimental activation cross-sections database of deuteron induced nuclear reactions on manganese up to 50 MeV. J. Radioanal. Nucl. Chem. 320(2019) 145-152 https://doi.org/10.1007/s10967-019-06423-x.
35. A. Hermanne, S. Takács, R. Adam-Rebeles, F. Tárkányi, M.P. Takács, New measurements and evaluation of database for deuteron induced reaction on Ni up to 50MeV. Nucl. Instruments Methods Phys. Res. Sect. B Beam Interact. with Mater. Atoms. 299(2013) 8-23 https://doi.org/10.1016/j.nimb.2013.01.005.
36. A.J. Koning, D. Rochman, Modern Nuclear Data Evaluation with the TALYS Code System. Nucl. Data Sheets. 113(2012) 2841-2934 https://doi.org/10.1016/J.NDS.2012.11.002.
37. N. Otuka, S. Takács, Corrigendum to: Definitions of radioisotope thick target yields. Radiochim. Acta. 106(2018) 875-875 https://doi.org/10.1515/ract-2013-9234.
38. P.P. Dmitriev, N.N. Krasnov, G.A. Molin, Yields of radioactive nuclides formed by bombardment of a thick target with 22-MeV deuterons. International Atomic Energy Agency (IAEA). 15(1983)
39. I.J. Gruverman, P. Kruger, Cyclotron-produced carrier-free radioisotopes. Int. J. appl. Radiat. Isotopes. 5(1959) 21-31 https://doi.org/10.1016/0020-708X(59)90347-3.
40. P.P. Dmitriev, I.O. Konstantinov, N.N. Krasnov, Methods for producing the Mn^{52} isotope. Soviet Atomic Energy. 26(1969) 539-541 https://doi.org/10.1007/BF01174115.